*Materials Research*. 2013; 16(5): 1092-1105
DOI: 10.1590/S1516-14392013005000091


# Effect of Temperatures and Strain Rates on the Average Size of Grains Refined by Dynamic Recrystallization for as-extruded 42CrMo Steel

***Guo-zheng Quan*, Yang Wang, ying-ying Liu, Jie Zhou***

*School of Material Science and Engineering, Chongqing University, Chongqing 400044, China*

Received: November 7, 2012; Revised: March 5, 2013

In order to study the dynamic recrystallization (DRX) behavior of as-extruded 42CrMo high-strength steel, a series of isothermal upsetting experiments were carried out in a temperature range of 1123~1348 K and a strain rate range of 0.01~10 $s^{-1}$ on Gleeble 1500. It was found that DRX softening is more recognizable at higher temperatures and lower strain rates, and stress level increases with increasing strain rate and decreasing deformation temperature. The types of flow stress evolution were distinguished by the following three characteristics: WH followed by DRX, WH followed by DRV, and WH followed by no dynamic softening. At a fixed temperature, the average grain size refined by DRX linearly decreases with increasing strain rate in log scale. At a fixed strain rate, the average grain size remains almost constant below 1273 K, while it rapidly increases above 1273 K. At a larger strain rate, data set of grain sizes has a smaller standard deviation to the average size value, and data have tightly grouped. This indicates that as strain rate increases, the microstructure becomes more and more uniform. The relationships between the average grain size and Zener-Hollomon parameter were nonlinearly fitted by the equation $D_A = 319.81202 - 13.6114 \ln Z + 0.15322 (\ln Z)^2$. The results from this equation show that the average grain size decreases with increasing Zener-Hollomon parameter. On the plot of $D_A$ versus ln*Z*, the regions corresponding to DRV (ln*Z* 37.8) and DRX (ln*Z* 37.8) were clarified clearly.

**Keywords:** *dynamic recrystallization, flow stress, microstructure, grain size*

## 1. Introduction

42CrMo (American grade: AISI 4140) is one of the representative medium carbon and low alloy steel. Due to its good balance of strength, toughness and wear resistance, 42CrMo high strength steel is widely used for many general purpose parts including automotive crankshaft, rams, spindles etc[1-3]. In the past, many investigations have been carried out on the behavior of 42CrMo steel[3-7]. Lin et al.[4] established the flow stress constitutive equations of 42CrMo steel describing the relationships of flow stress, strain rate and temperature. Kim et al.[7] investigate the effect of deformation mode on constitutive relations for 42CrMo steel by hot torsion and compression tests. Lin et al.[8] investigated the effects of processing parameters including strain rate, temperature and deformation degree on the microstructures of 42CrMo steel. Kim and Yoo[9] established the quantitative relationships between flow stress and the volume fraction of dynamic recrystallization (DRX) as a function of processing variables such as strain rate, temperature and strain for 42CrMo steel, by means of torsion tests. Quan et al.[10] investigated the relationships between processing variables and DRX volume fraction for 42CrMo steel, and the evolutions of DRX volume was described by the modified Avrami type equation. A large amount of efforts have been paid to the constitutive modeling of the flow behavior of 42CrMo steel, and only a few attentions have been paid to the constitutive modeling of DRX kinetics. However, there isn't any report about the constitutive modeling of the relationships between average grain size and deformation conditions.

In the present work, the critical stress for DRX initiation has been identified from WH rate versus stress curves of as-extruded 42CrMo high-strength steel, and its existence means the occurence of DRX. The object of this study is to exhibit the microstructure evolution by a series of metallographs, uncover the flow stress softening mechanisms including DRX and dynamic recovery (DRV), and then describe the general nature of the influence of strain rate and temperature on the average size of grains refined by DRX. The effects of temperature and strain rate on the average grain size are represented by Zener-Hollomon parameter, *Z*, in an exponent-type function of temperature and strain rate. Then the relationships between the average grain size and Zener-Hollomon parameter were nonlinearly fitted by the equation $D_A = 319.81202 - 13.6114 \ln Z + 0.15322 (\ln Z)^2$. In further, on the plot of $D_A$ versus ln*Z*, the regions corresponding to DRV (ln*Z* 37.8) and DRX (ln*Z* 37.8) were clarified.

## 2. Materials and Experimental Methods

The chemical composition (wt.%) of as-extruded 42CrMo high-strength steel used in this study is as follows: C-0.450, Si-0.280, Cr-0.960, Mn-0.630, Mo-0.190, P-0.016, Cu-0.014, S-0.012, and the rest Fe[1]. Then the rod was cut

*e-mail: quanguozheng@cqu.edu.cn

into specimens of diameter 10 mm and height 12 mm with grooves on both sides filled with machine oil mingled with graphite powder as lubricant to reduce friction between the anvils and specimen. The schematic representation of the specimen before and after the uniaxial compression testing is shown in Figure 1a and b, respectively. Seventeen such cylindrical specimens were prepared. A computer-controlled, servo-hydraulic Gleeble 1500 machine was used for compression testing. The specimens were resistance heated to the deformation temperature at a heating rate of 10 K/s and held at that temperature for 300 s by thermo-coupled-feedback-controlled AC current. One specimen was considered as the as-received specimen, which was not heated and compressed for the observation of original microstructure. Sixteen specimens were compressed with a height reduction of 60% at four different temperatures of 1123 K, 1198 K, 1273 K, 1348 K and four different strain rates of 0.01 $s^{-1}$, 0.1 $s^{-1}$, 1 $s^{-1}$, 10 $s^{-1}$. After each compression, the deformed specimens were rapidly quenched with water to retain the recrystallized microstructures. Then all the samples were sectioned along the longitudinal compression axis for metallographic examination. The microstructures were examined in the center zone of the specimens (marked "X" in Figure 1b). The sections were polished and etched in an ablument solution of saturated picric acid. The optical microstructures in the center region of the section plane were examined.

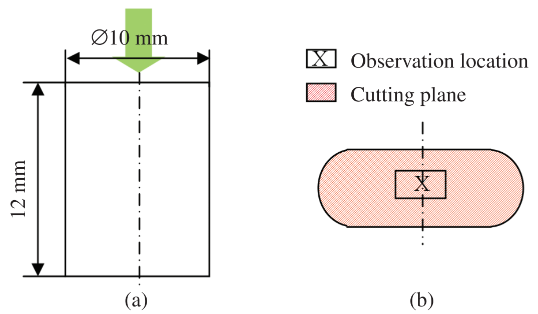


**Figure 1.** Schematic representation of the uniaxial compression specimen (a) before (arrow indicates the applied load direction) and (b) after the testing (section with hatch pattern shows the cut plane, and region marked "X" indicates the observation location).

During the compression process, the variations of stress and strain were monitored continuously by a personal

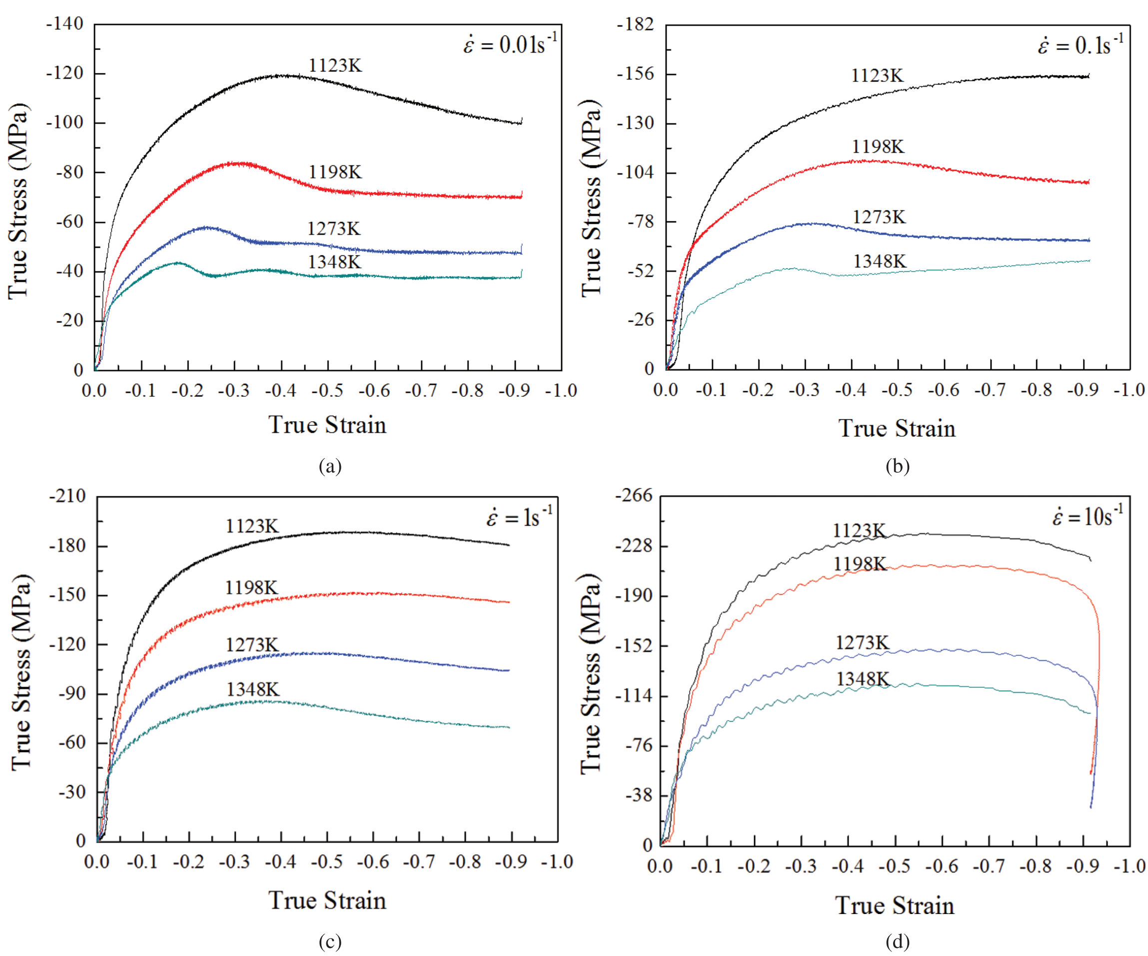


**Figure 2.** True stress-strain curves of as-extruded 42CrMo high-strength steel obtained by Gleeble 1500 under the different deformation temperatures with strain rates. (a) 0.01 $s^{-1}$, (b) 0.1 $s^{-1}$, (c) 1 $s^{-1}$, (d) 10 $s^{-1}$.

computer equipped with an automatic data acquisition system. The true stress and true strain were derived from the measurement of nominal stress-strain relationship according to the following formula: $\sigma_T = \sigma_N(1+\varepsilon_N)$, $\varepsilon_T = \ln(1+\varepsilon_N)$, where $\sigma_T$ is the true stress, $\sigma_N$ is the nominal strain, $\varepsilon_T$ is the true strain and $\varepsilon_N$ is the nominal strain[11].

## 3. Results and Dissuction

### 3.1. *Characteristics of softening flow behavior coupling with DRX*

The true stress-strain data were shown in Figure 2a-d. From the aforementioned stress-strain curves, it was summarized that the work-hardening (WH) effect is pronounced at higher strain rate and lower temperature, while at higher temperature and lower strain rate, the strain softening effect is pronounced. In order to improve the understanding of the flow behavior, the analysis of WH rate is essential. In order to obtain the WH rate the stress-strain data in Figure 2a-d were analyzed by fitting each experimental curve with a polynomial expression and taking its derivative with respect to strain. Then, the WH rate ($\theta = d\sigma/d\varepsilon$) was plotted against flow stress ($\sigma$) as shown in Figure 3a-d. For a given strain, the WH rate is the derivative of stress with respect to strain ($\varepsilon$), which corresponds to the tangent at this strain value. From all the $\theta$ versus $\sigma$ curves in Figure 3a-d, it can be summarized that the stress evolution with strain obviously exhibits three distinct stages. In the first and the second stages, $\theta$-values are positive which indicates WH characteristics. While, in the third stage, $\theta$-values exhibit three types of variation tendency such as negative variables with $\sigma$, almost positive constants, and positive increasing variables. Negative variables represent the predominance of DRX softening. Positive constants represent balance between dominant DRV softening and WH. Positive increasing variables represent the predominance of WH. In further, the types of flow stress evolution were distinguished by the following three characteristics: WH followed by DRX, WH followed by DRV, and WH followed by no dynamic softening.

At the first stage where work hardening (WH) predominates, flow stress exhibits a rapid increase (i.e. relatively large positive $\theta$-value) to a critical value ($\sigma_C$) with increasing strain, meanwhile the stored energy in the grain boundaries originates from a large difference in dislocation density within subgrains or grains and grows rapidly to DRX activation energy. When the critical driving

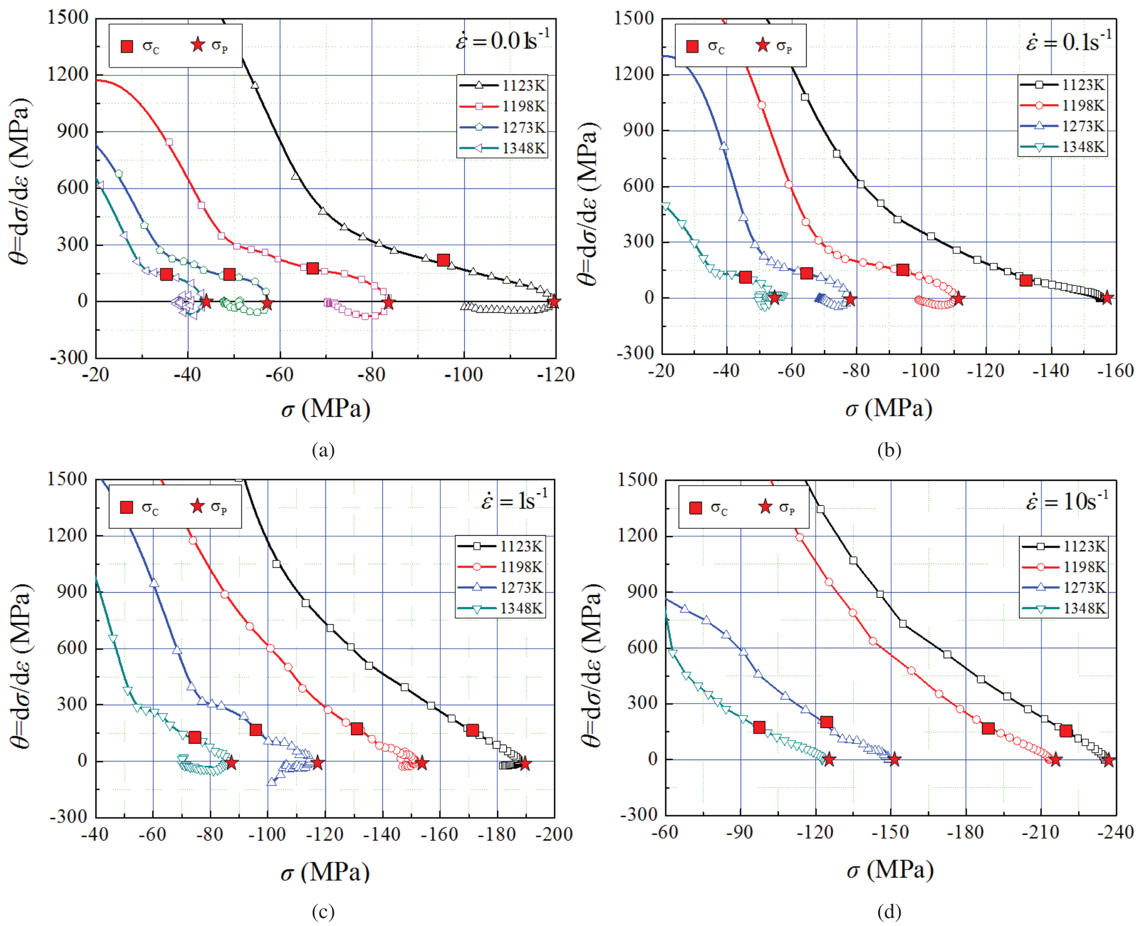


**Figure 3.** $\theta = d\sigma/d\varepsilon$ versus $\sigma$ plots under different deformation temperatures with strain rates (a) 0.01 $s^{-1}$, (b) 0.1 $s^{-1}$, (c) 1 $s^{-1}$, (d) 10 $s^{-1}$.

force is attained, new grains are nucleated along the grain boundaries, deformation bands and dislocations, resulting in equiaxed DRX grains. At the second stage, flow stress exhibits a smaller and smaller increase until a peak value ($\sigma_p$) with a relatively small positive $\theta$-value. At the beginning of the second stage, the critical driving force of DRX has been attained, and then new equiaxed grains are nucleated along the original grain boundaries. The onset of DRX softening mechanism induces an obvious inflection of WH rate. At the third stage, as $\sigma$-value decreases below $\sigma_p$, $\theta$-value becomes negative, which means that the thermal softening exceeds work hardening and becomes predominant. At this stage, three types of $\theta$ versus $\sigma$ curve variation tendency can be generalized as follows. As for the first type corresponding to the deformation conditions of 1123~1348 K & 0.01 $s^{-1}$, 1198~1348 K & 0.1 $s^{-1}$, 1273~1348 K & 1 $s^{-1}$, $\theta$-value increases up to the negative peak which corresponds to a valley point of $\theta$ versus $\sigma$ plot, and then, $\theta$-value decreases to zero which corresponds to the onset of a steady state flow as a plateau (a balance between dominant DRX softening and WH) in stress-strain curve. As for the second type corresponding to the deformation conditions of 1123~1198 K & 1 $s^{-1}$, 1123~1348 K & 10 $s^{-1}$, $\theta$-value always maintains a steady state which indicates the balance between dominant DRV softening and WH. As for the third type corresponding to the deformation condition of 1123 K & 0.1 $s^{-1}$, $\theta$-value increases continuously which indicates significant WH.

The analysis after the hot compression tests reveals that during the hot forming process with a temperature range of 1123~1348 K, a strain rate range of 0.01~10 $s^{-1}$, and a true strain range of 0~ –0.9, as-extruded 42CrMo high-strength steel is liable to undergo WH, DRV and DRX, three metallurgical phenomena for controlling microstructure and mechanical properties. DRV induces the fact that flow stress saturates after an initial period of work hardening. This saturation value depends on temperature, strain rate and composition. During DRV, the original grains get increasingly strained, but the sub-boundaries remain more or less equiaxed. This implies that the substructure is 'dynamic' and readapts continuously to the increasing strain. At a critical strain, and correspondingly at a value/variation in driving force, dynamically recrystallized grains appear at the original grain boundaries, which results in the so-called 'necklace structure'[12,13]. With further deformation, more and more potential nuclei are activated and new recrystallized grains appear[14,15]. At the same time, the grains, which had already recrystallized in a previous stage, are deformed again. After a certain amount of strain, typical equilibrium is reached between the hardening due to dislocation accumulation and the softening due to DRX. At this stage, the flow curve reaches a plateau, and the microstructure consists of a dynamic mixture of grains with various dislocation densities[10].

## 3.2. *Microstructure observation*

The frozen microstructures on the section plane of specimen deformed to the true strain of –0.9 were examined under the optical microscope. Figure 4 shows the as-received microstructure of as-extruded 42CrMo high-strength steel specimen with a single-phase FCC structure and a homogeneous aggregate of rough equiaxed polygonal grains, while with negligible volume fraction of inclusions or second-phase precipitates. The grain boundaries are straight to gently curved and often intersect at ~120° triple junctions. Figure 5a-d show the typical microstructures of the specimens of as-extruded 42CrMo high-strength steel deformed to a strain of –0.9 at the temperature of 1123 K and at the strain rates of 0.01 $s^{-1}$, 0.1 $s^{-1}$, 1 $s^{-1}$ and 10 $s^{-1}$, respectively. Figure 6a-d show the typical microstructures of the specimens of as-extruded 42CrMo high-strength steel deformed to a strain of –0.9 at the temperature of 1198 K and at the strain rates of 0.01 $s^{-1}$, 0.1 $s^{-1}$, 1 $s^{-1}$ and 10 $s^{-1}$, respectively. Figure 7a-d show the typical microstructures of the specimens of as-extruded 42CrMo high-strength steel deformed to a strain of –0.9 at the temperature of 1273 K and at the strain rates of 0.01 $s^{-1}$, 0.1 $s^{-1}$, 1 $s^{-1}$ and 10 $s^{-1}$, respectively. Figure 8a-d show the typical microstructures of the specimens of as-extruded 42CrMo high-strength steel deformed to a strain of -0.9 at the temperature of 1348 K and at the strain rates of 0.01 $s^{-1}$, 0.1 $s^{-1}$, 1 $s^{-1}$ and 10 $s^{-1}$, respectively.

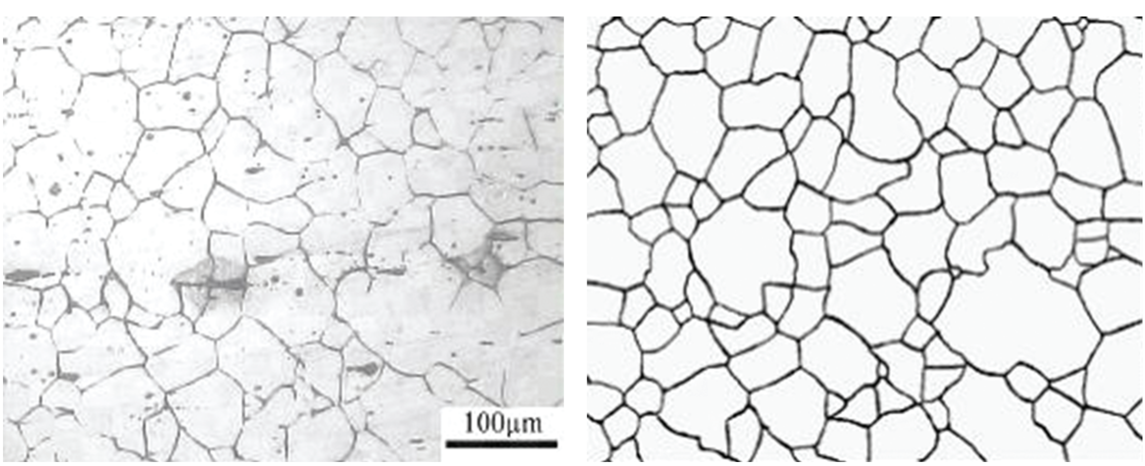


**Figure 4.** Optical microstructures and average grain size of as-extruded 42CrMo high-strength steel undeformed (starting material).

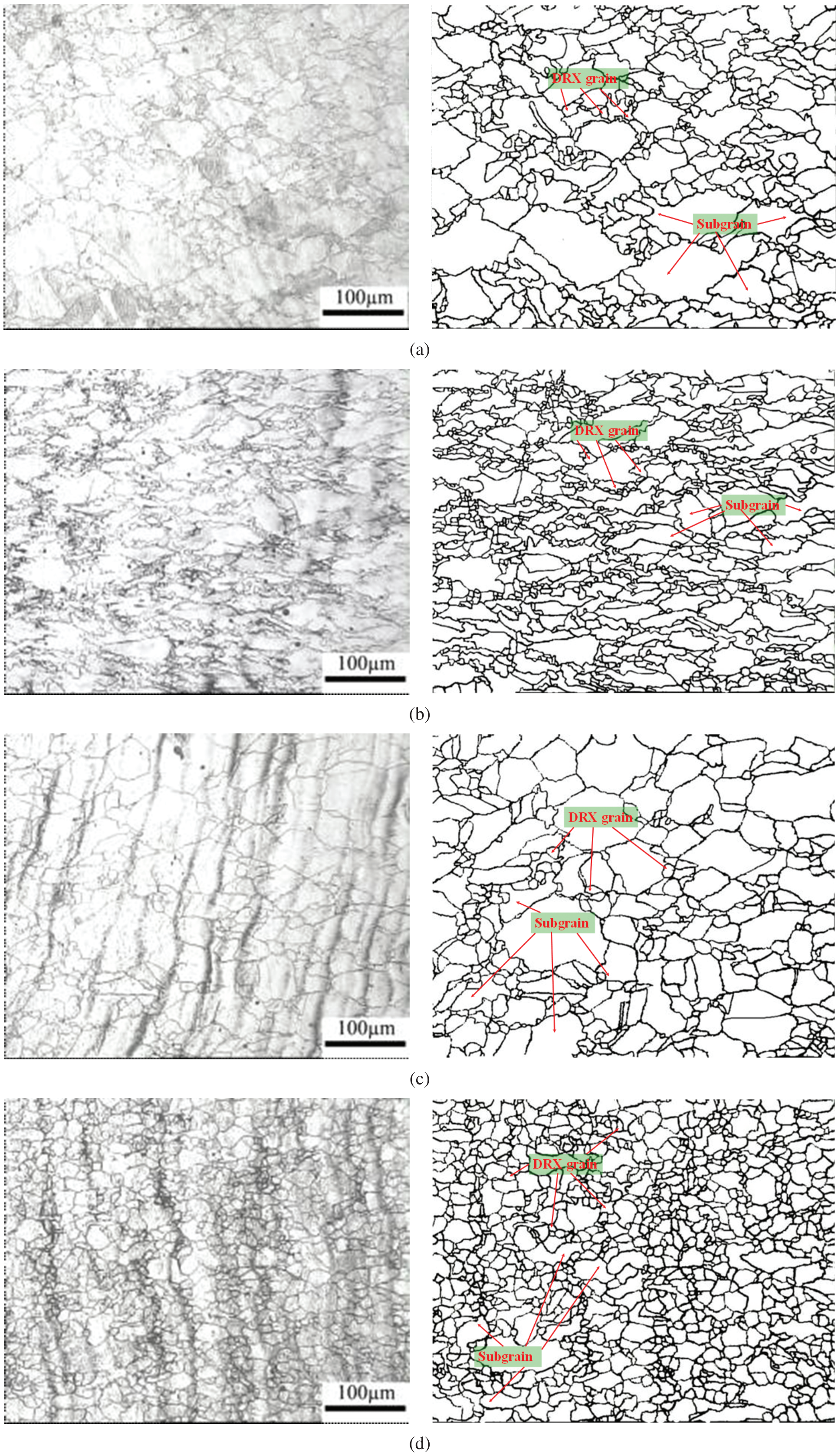


**Figure 5.** Optical microstructures of as-extruded 42CrMo high-strength steel at a fix true strain of –0.9, a fix temperature of 1123 K and different strain rates: (a) 0.01 $s^{-1}$, (b) 0.1 $s^{-1}$, (c) 1 $s^{-1}$, (d) 10 $s^{-1}$.

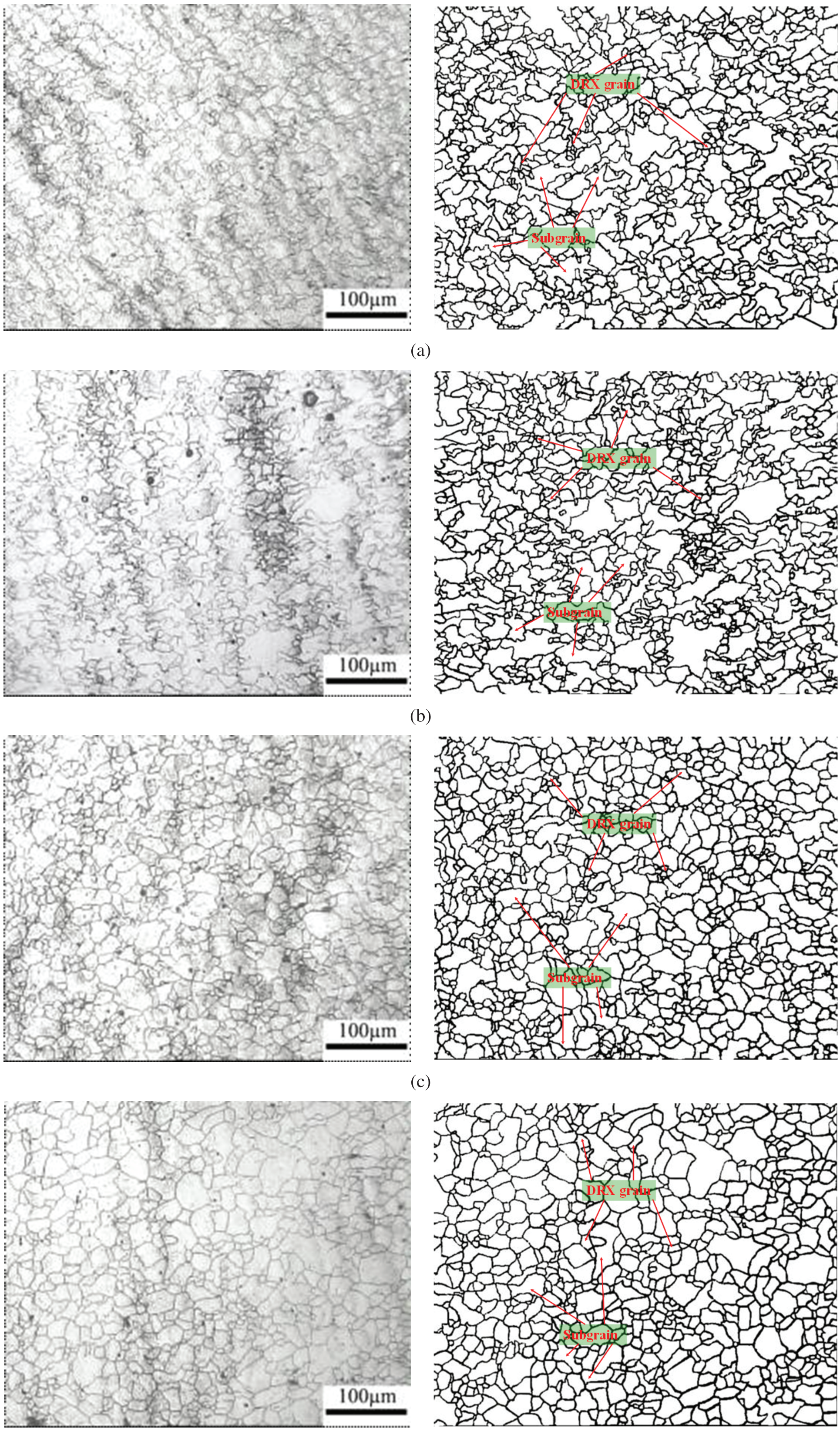


**Figure 6.** Optical microstructures of as-extruded 42CrMo high-strength steel at a fix true strain of –0.9, a fix temperature of 1198 K and different strain rates: (a) 0.01 $s^{-1}$, (b) 0.1 $s^{-1}$, (c) 1 $s^{-1}$, (d) 10 $s^{-1}$.

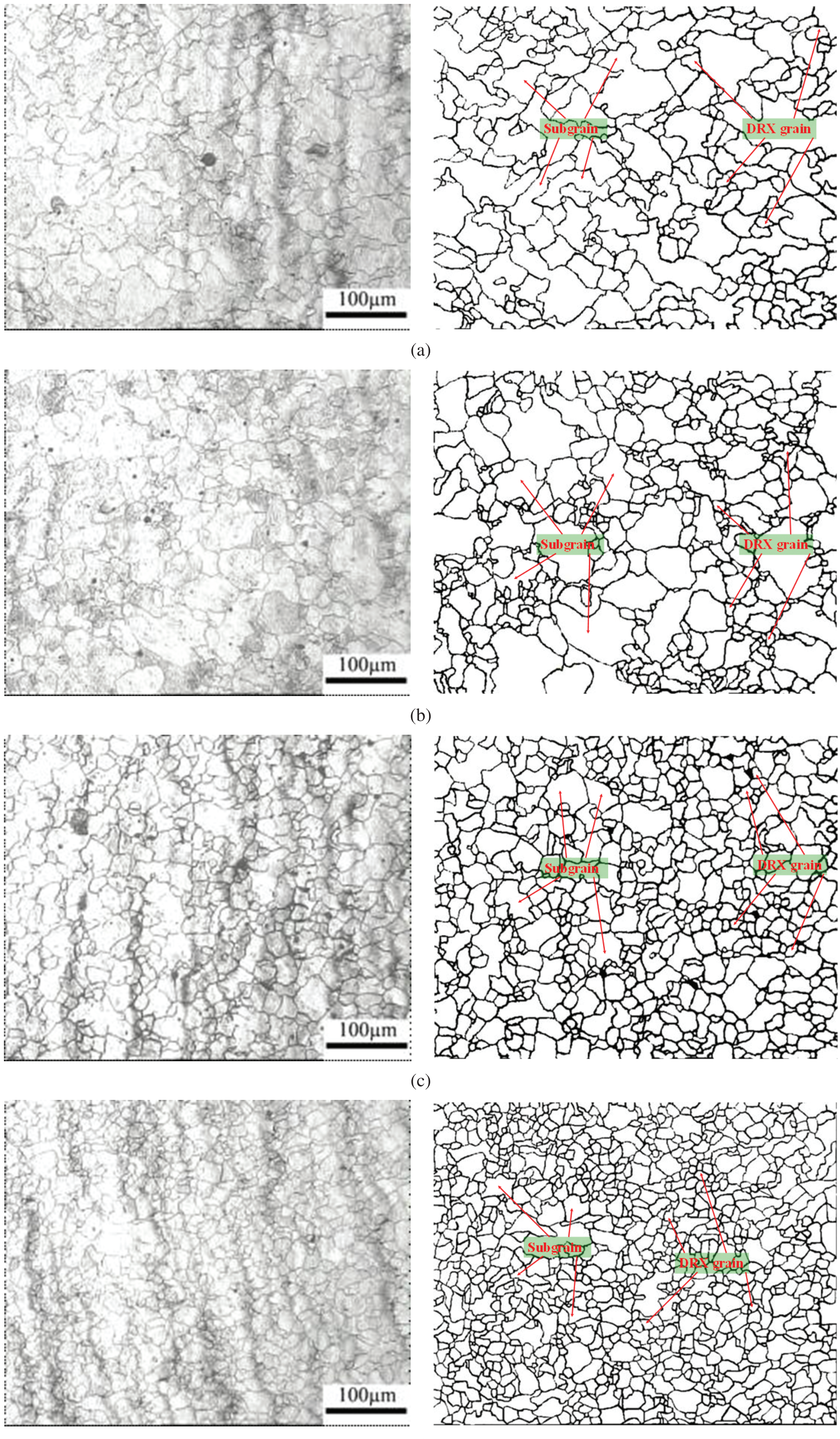


**Figure 7.** Optical microstructures of as-extruded 42CrMo high-strength steel at a fix true strain of –0.9, a fix temperature of 1273 K and different strain rates: (a) 0.01 $s^{-1}$, (b) 0.1 $s^{-1}$, (c) 1 $s^{-1}$, (d) 10 $s^{-1}$.

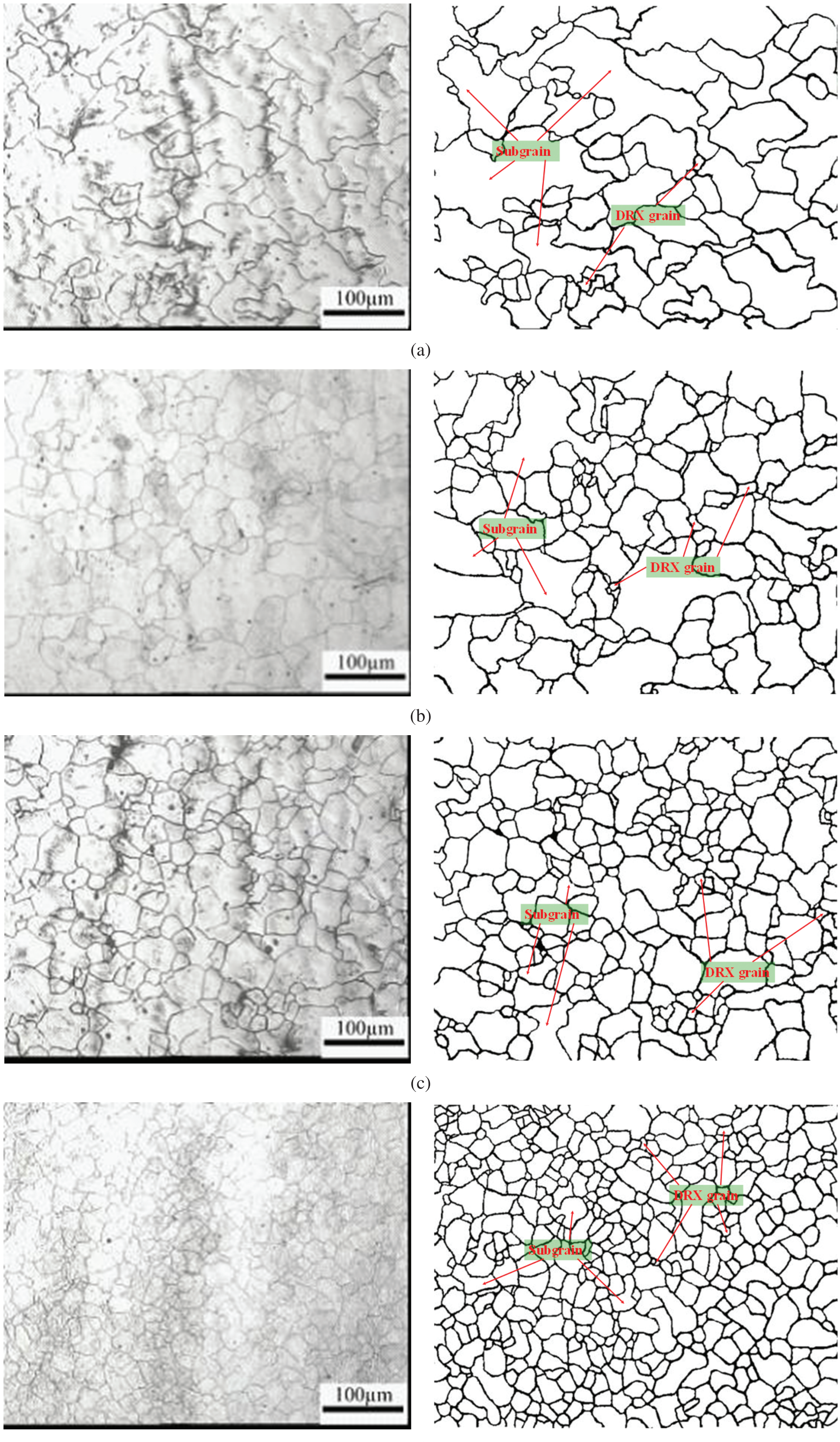


**Figure 8.** Optical microstructures of as-extruded 42CrMo high-strength steel at a fix true strain of –0.9, a fix temperature of 1348 K and different strain rates: (a) 0.01 $s^{-1}$, (b) 0.1 $s^{-1}$, (c) 1 $s^{-1}$, (d) 10 $s^{-1}$.

At such deformation conditions the recrystallized grains with wavy or corrugated grain boundaries can be easily identified from subgrains by the misorientation between adjacent grains, i.e. subgrains are surrounded by low angle boundaries while recrystallized grains have high angle boundaries. In Figure 5-8 a part of subgrains and DRX grains have been marked. From Figure 5-8 it can be seen that the deformed metal completely or partially transforms to a microstructure of approximately equiaxed defect-free grains which are predominantly bounded by high angle boundaries (i.e. a recrystallized microstructure). The results of microstructure observation imply the levels of dynamically recrystallized volume fractions, and such levels can be roughly and indirectly estimated by the following statistical analysis of the average grain size due to the fact that smaller average grain size means larger volume fraction of DRX as DRX makes the original equiaxed grains refined.

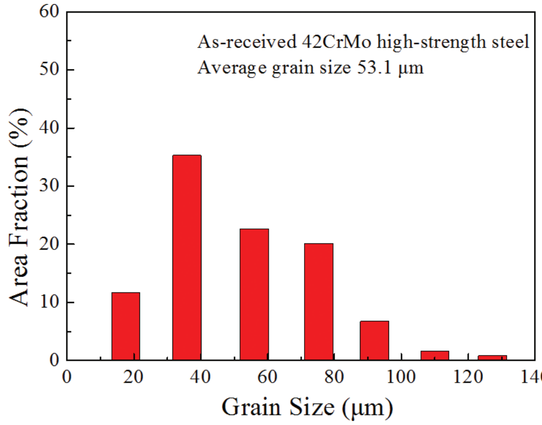


**Figure 9.** Grain size distribution of as-extruded 42CrMo high-strength steel undeformed (starting material).

## 3.3. *Effect of temperatures and strain rates on average grain size*

Figure 9 shows the grain size distribution of as-extruded 42CrMo high-strength steel undeformed (starting material). Figure 10 shows the effects of the strain rate on the grain size distribution of as-extruded 42CrMo high-strength steel under the true strain of –0.9 and temperature of 1123 K. Figure 11 shows the effects of the strain rate on the grain size distribution of as-extruded 42CrMo high-strength steel under the true strain of –0.9 and temperature of 1198 K.

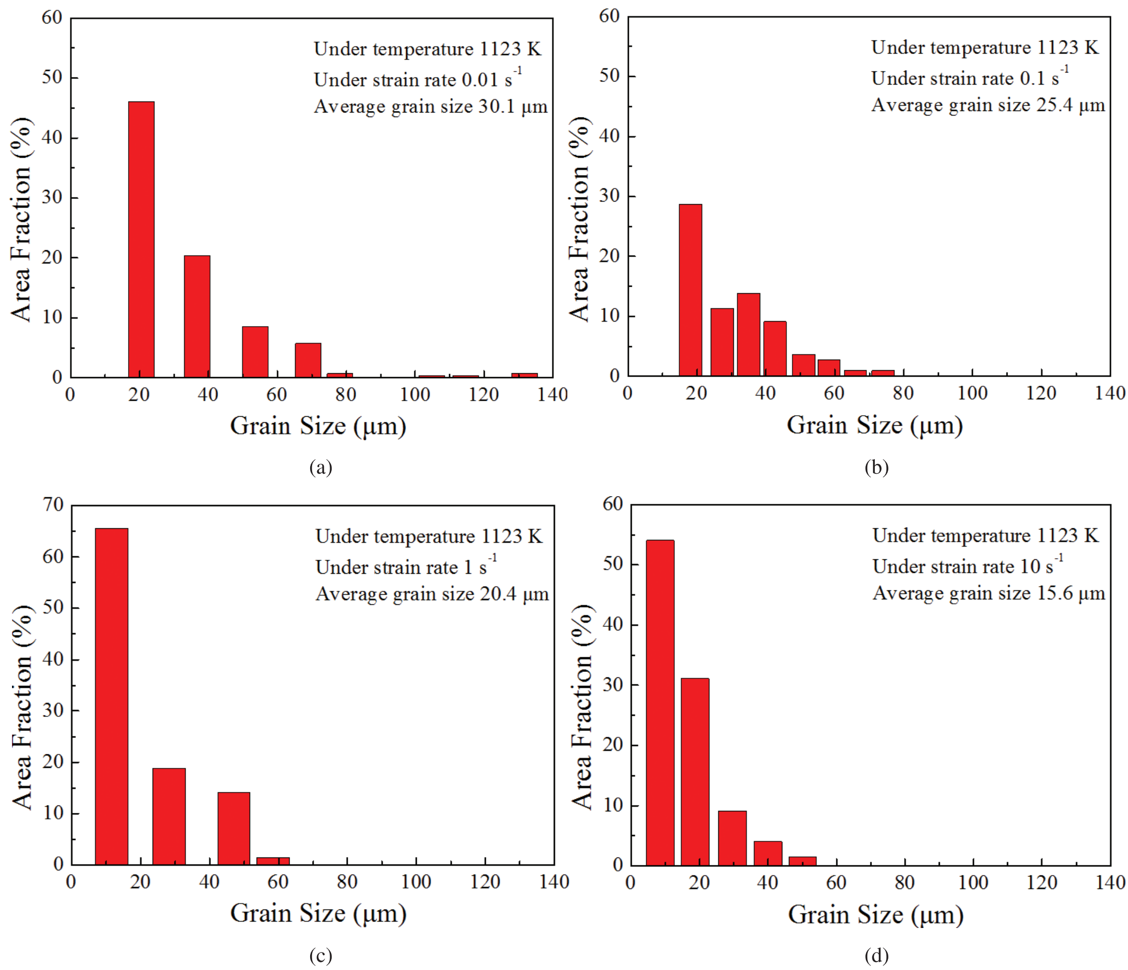


**Figure 10.** Grain size distribution of 42CrMo high-strength steel at a fix true strain of –0.9, a fix temperature of 1123 K and different strain rates: (a) 0.01 $s^{-1}$, (b) 0.1 $s^{-1}$, (c) 1 $s^{-1}$, (d) 10 $s^{-1}$.

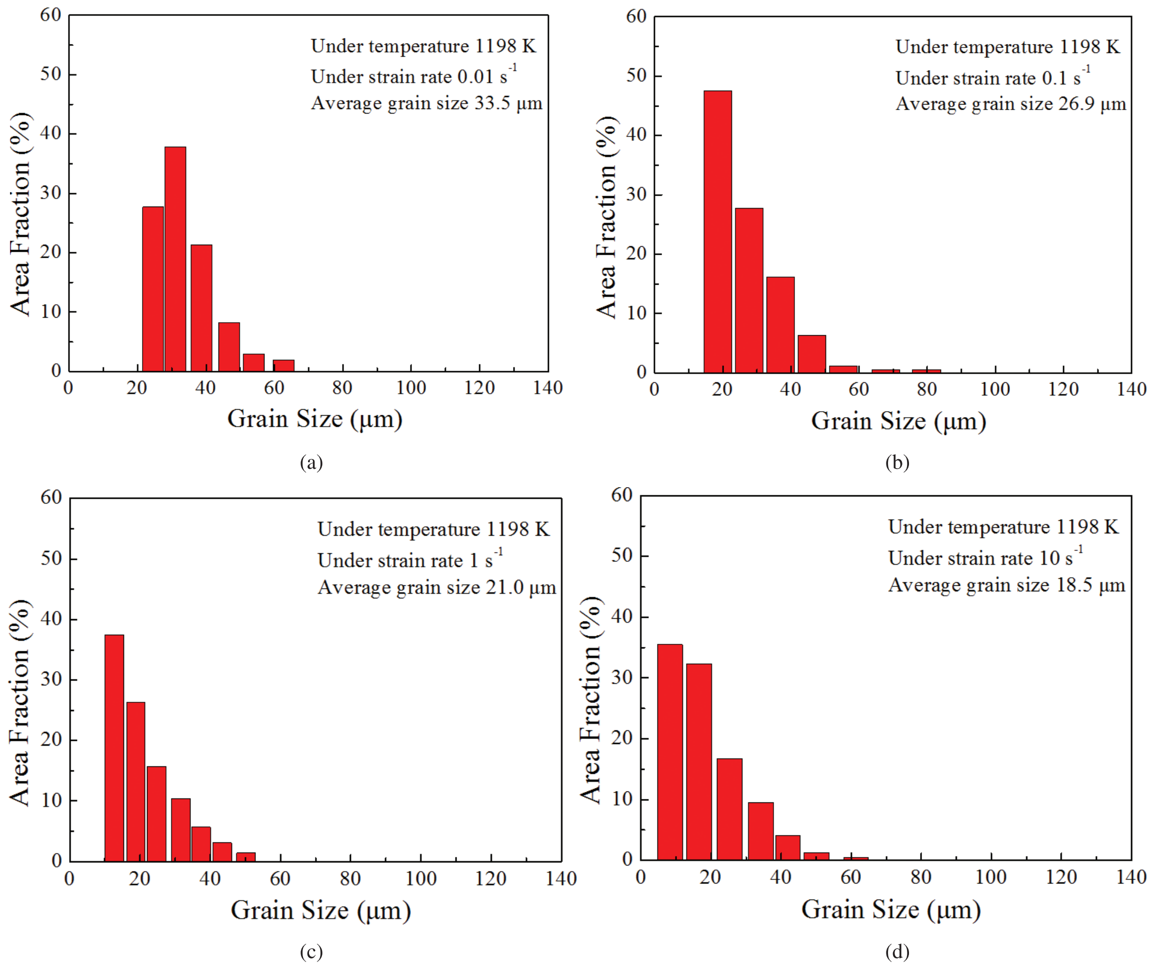


**Figure 11.** Grain size distribution of 42CrMo high-strength steel at a fix true strain of –0.9, a fix temperature of 1198 K and different strain rates: (a) 0.01 $s^{-1}$, (b) 0.1 $s^{-1}$, (c) 1 $s^{-1}$, (d) 10 $s^{-1}$.

Figure 12 shows the effects of the strain rate on the grain size distribution of as-extruded 42CrMo high-strength steel under the true strain of –0.9 and temperature of 1273 K. Figure 13 shows the effects of the strain rate on the grain size distribution of as-extruded 42CrMo high-strength steel under the true strain of –0.9 and temperature of 1348 K.

As depicted, under a fix temperature of 1123 K the microstructure of the as-extruded billet with grain size of 53.1 μm became refined up to about 30.1 μm after upsetting under strain rate 0.01 $s^{-1}$, to about 25.4 μm under strain rate 0.1 $s^{-1}$, to about 20.4 μm under strain rate 1 $s^{-1}$, to about 15.6 μm under strain rate 10 $s^{-1}$. Under a fix temperature of 1198 K the microstructure of the as-extruded billet with grain size of 53.1 μm became refined up to about 33.5 μm after upsetting under strain rate 0.01 $s^{-1}$, to about 26.9 μm under strain rate 0.1 $s^{-1}$, to about 21.0 μm under strain rate 1 $s^{-1}$, to about 18.5 μm under strain rate 10 $s^{-1}$. Under a fix temperature of 1273 K the microstructure of the as-extruded billet with grain size of 53.1 μm became refined up to about 33.5 μm after upsetting under strain rate 0.01 $s^{-1}$, to about 27.3 μm under strain rate 0.1 $s^{-1}$, to about 19.7 μm under strain rate 1 $s^{-1}$, to about 15.7 μm under strain rate 10 $s^{-1}$. Under a fix temperature of 1348 K the microstructure of the as-extruded billet with grain size of 53.1 μm became refined up to about 49.8 μm after upsetting under strain rate 0.01 $s^{-1}$, to about 38.2 μm under strain rate 0.1 $s^{-1}$, to about 32.2 μm under strain rate 1 $s^{-1}$, to about 24.4 μm under strain rate 10 $s^{-1}$. It can be summarized that under a fix temperature, as strain rate increases, the microstructure becomes more and more refined due to increasing stored energy (i.e. high nucleation rate) and decreasing grain growth time[16]. Lin et al.[8] investigated the effects of processing parameters including strain rate, temperature on the microstructures of 42CrMo steel by metallurgical analysis. The results show that the average grain size of the deformed 42CrMo steel increases with temperature and decreases with strain rate. In our work, the same conclusion has been achieved.

In Figure 9, it can be seen that as for the starting material, the area fraction of large grains with size greater than 56 μm is about 51%, and the area fraction of finer grains with size less than 30 μm is about 12%. In Figure 10 corresponding to a fix temperature of 1123 K and different strain rates of 0.01 $s^{-1}$, 0.1 $s^{-1}$, 1 $s^{-1}$ and 10 $s^{-1}$, the area

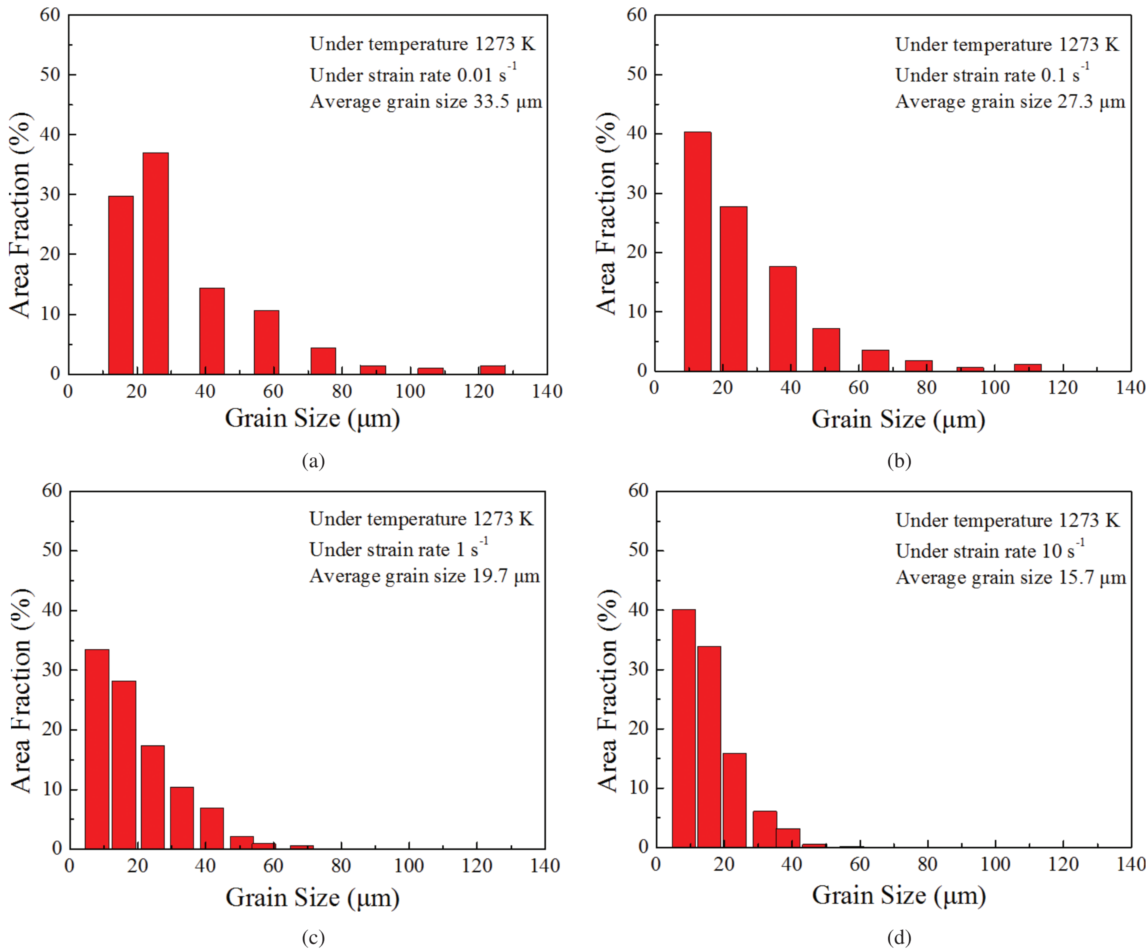


**Figure 12.** Grain size distribution of 42CrMo high-strength steel at a fix true strain of –0.9, a fix temperature of 1273 K and different strain rates: (a) 0.01 $s^{-1}$, (b) 0.1 $s^{-1}$, (c) 1 $s^{-1}$, (d) 10 $s^{-1}$.

fraction 51% of large grains with size greater than 56 μm after upsetting has decreased to about 14%, 7%, 2% and 1% respectively, meanwhile the area fraction 12% of the finer grain with size less than 30 μm after upsetting has increased up to 46%, 54%, 83% and 92% respectively. In Figure 11 corresponding to a fix temperature of 1198 K and different strain rates of 0.01 $s^{-1}$, 0.1 $s^{-1}$, 1 $s^{-1}$ and 10 $s^{-1}$, the area fraction 51% of large grains with size greater than 56 μm after upsetting has decreased to about 4%, 2%, 0% and 1% respectively, meanwhile the area fraction 12% of the finer grain with size less than 30 μm after upsetting has increased up to 65%, 75%, 78% and 83% respectively. In Figure 12 corresponding to a fix temperature of 1273 K and different strain rates of 0.01 $s^{-1}$, 0.1 $s^{-1}$, 1 $s^{-1}$ and 10 $s^{-1}$, the area fraction 51% of large grains with size greater than 56 μm after upsetting has decreased to about 18%, 7%, 1% and 0% respectively, meanwhile the area fraction 12% of the finer grain with size less than 30 μm after upsetting has increased up to 66%, 68%, 80% and 90% respectively. In Figure 13 corresponding to a fix temperature of 1348 K and different strain rates of 0.01 $s^{-1}$, 0.1 $s^{-1}$, 1 $s^{-1}$ and 10 $s^{-1}$, the area fraction 51% of large grains with size greater than 56 μm after upsetting has decreased to about 42%, 33%, 10% and 2% respectively, meanwhile the area fraction 12% of the finer grain with size less than 30 μm after upsetting has increased up to 30%, 39%, 47% and 64% respectively. From the above detailed description, it can be concluded that under a fix temperature, as deformation strain rate increases, the area fraction of large grains becomes smaller and smaller, meanwhile the area fraction of finer grains becomes larger and larger. It is obvious that at a lower strain rate, data set of grain sizes has a larger standard deviation to the average size value, and data spread out over a wide range of values. However, at a larger strain rate, data set of grain sizes has a smaller standard deviation to the average size value, and data have tightly grouped. In further, it can be deduced that as strain rate increases, the microstructure becomes more and more uniform.

In this work, the changes in the average grain size according to deformation temperature and strain rate are shown in Figure 14a, b. As shown in Figure 14a, the average grain size refined by DRX linearly decreases with increasing strain rate (in log scale). Under higher strain rates, samples preserve a majority of deformation energy, which results in high nucleation rates of recrystallization grains. For a fixed temperature, higher strain rate means that the recrystallized grains have no enough growth time. Thus more refined grains will be achieved. As shown in Figure 14b, the average grain size refined by DRX remains almost constant below 1273 K, while it rapidly increases above 1273 K. This indicates that grain growth is not predominant below 1273K while it is significant above 1273 K.

### 3.4. *Modeling of grain size evolution*

It is generally believed that average grain size ($D_A$) decreases with increasing strain rate and decreasing temperature, and is independent of initial grain size and accumulated strain. The effects of temperature and strain rate

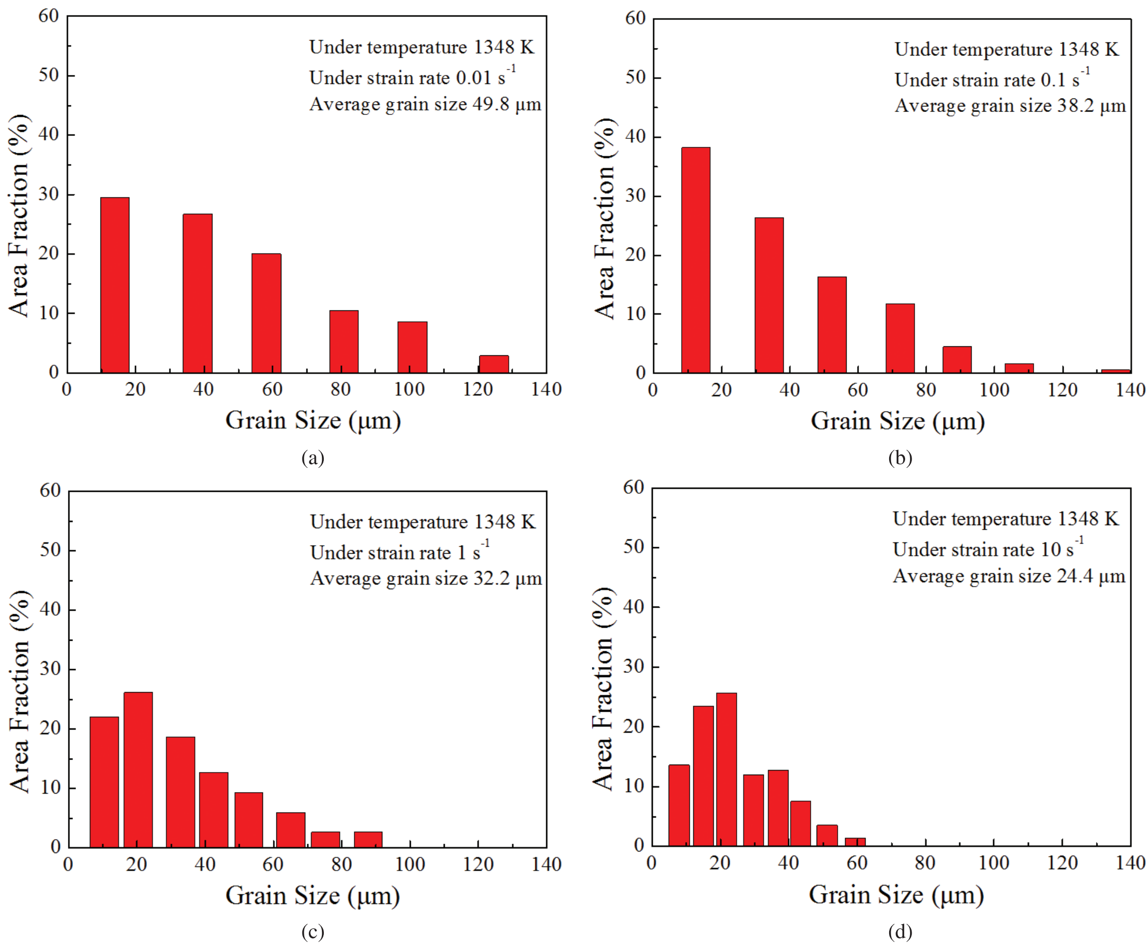


**Figure 13.** Grain size distribution of 42CrMo high-strength steel at a fix true strain of –0.9, a fix temperature of 1348 K and different strain rates: (a) 0.01 s$^{-1}$, (b) 0.1 s$^{-1}$, (c) 1 s$^{-1}$, (d) 10 s$^{-1}$.

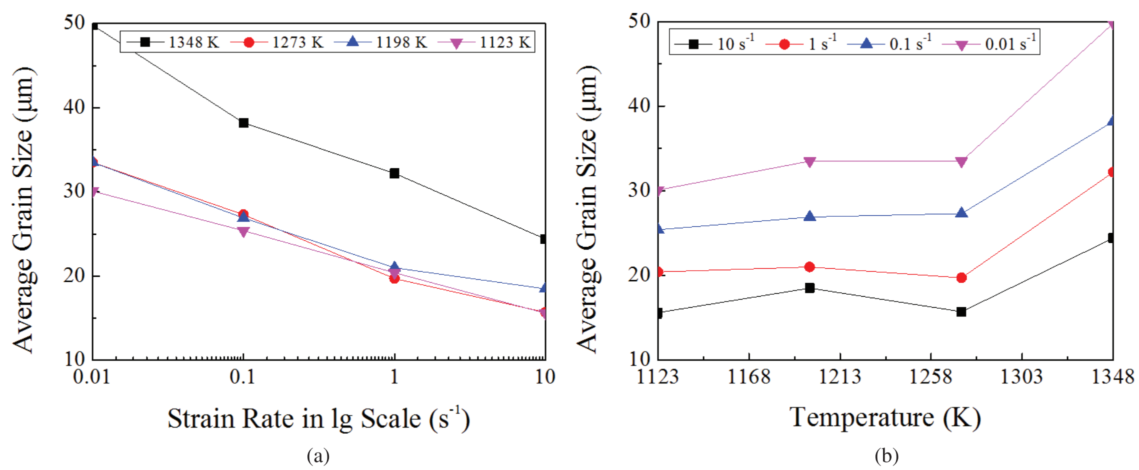


**Figure 14.** Changes in average grain size according to (a) strain rate, (b) temperature.

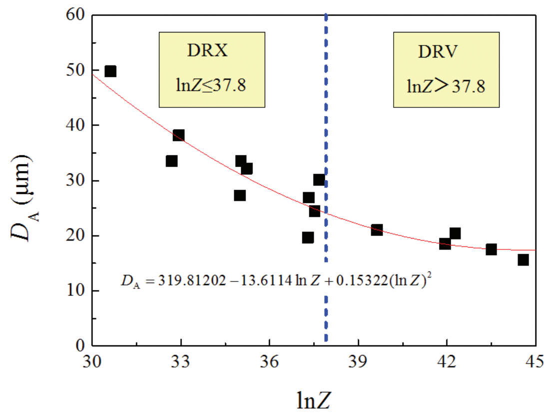


**Figure 15.** Relationships between average grain size $D_A$ (μm) and *Z* parameter.

can be expressed in terms of the second-order function of Zener-Hollomon parameter, *Z*, in an exponent-type function of temperature and strain rate, as following[17-19]:

$$D_A = B_0 + B_1 \ln Z + B_2 (\ln Z)^2$$

where $B_1$ and $B_2$ are polynomial coefficients.

In this work, the variations of average grain size according to different temperatures and strain rates have been achieved. By taking all these results into consideration and an overall analysis, $B_1$ and $B_2$ are determined by regression analysis as $B_0 = 319.81202$, $B_1 = -13.6114$ and $B_2 = 0.15322$. Therefore, the formula of average grain size for as-extruded 42CrMo high-strength steel is described as following:

$$D_A = 319.81202 - 13.6114 \ln Z + 0.15322 (\ln Z)^2 \text{ (μm)}$$

which can be used to predict and control the recrystallized grain size of as-extruded 42CrMo high-strength steel after hot deformation. Figure 15 shows the evolution of average grain size according to lnZ. It is obvious that the average grain size $D_A$ (μm) decreases with *Z* parameter rising. According to the description of softening flow behaviors in Section 3.1, DRX softening is predominant in the deformation parameter window of 1123~1348 K & 0.01 $s^{-1}$, 1198~1348 K & 0.1 $s^{-1}$ and 1273~1348 K & 1 $s^{-1}$, while DRV softening is predominant in the deformation parameter window of 1123~1198 K & 1 $s^{-1}$ and 1123~1348 K & 10 $s^{-1}$. In accordance with the different windows, two regions can be clarified: $\ln Z \le 37.8$ for DRX region, $\ln Z > 37.8$ for DRV region. However, the point corresponding to the deformation condition of 1123 K & 0.1 $s^{-1}$ doesn't appear in DRX region or DRV region in Figure 14 because under such condition, WH is followed by no dynamic softening.

## 4. Conclusions

The deformation characteristics of as-extruded 42CrMo high-strength steel by means of hot compression tests have been investigated in the temperature range of 1123~1348 K and the strain rate range of 0.01~10 $s^{-1}$. The results are listed below:

- A typical flow stress curve with DRX is more recognizable at higher temperatures and lower strain rates, and the flow stress level increases with increasing strain rate and decreasing deformation temperature. The types of flow stress evolution were distinguished by the following three characteristics: WH followed by DRX, WH followed by DRV, and WH followed by no dynamic softening;
- At a fixed temperature, the average grain size refined by DRX linearly decreases with increasing strain rate (in log scale). At a fixed strain rate, the average grain size refined by DRX remains almost constant below 1273 K, while it rapidly increases above 1273 K;
- At a lower strain rate, data set of grain sizes has a larger standard deviation to the average size value, and data spread out over a wide range of values. However, at a larger strain rate, data set of grain sizes has a smaller standard deviation to the average size value, and data have tightly grouped. As strain rate increases, the microstructure becomes more and more uniform;
- The relationships between average grain size and ln*Z* were expressed by the equation: $D_A = 319.81202 - 13.6114 \ln Z + 0.15322 (\ln Z)^2$ (μm), and the average grain size of as-extruded 42CrMo high-strength steel decreases with the increase of Zener– Hollomon parameter. The regions corresponding to DRV ($\ln Z > 37.8$) and DRX ($\ln Z \le 37.8$) have been clarified by *Z* values.


## Acknowledgements

This work was supported by Fundamental Research Funds for the Central Universities (CDJZR11130009).


## References


1. Quan GZ, Tong Y, Luo G and Zhou J. A characterization for the flow behavior of 42CrMo steel. *Computational Materials Science*. 2010; 50(1):167-171. http://dx.doi.org/10.1016/j.commatsci.2010.07.021
2. Lin YC and Chen X-M. A critical review of experimental results and constitutive descriptions for metals in hot working. *Materials & Design*. 2011; 32(4):1733-1759. http://dx.doi.org/10.1016/j.matdes.2010.11.048
3. Lin YC, Chen MS and Zhong J. Numerical simulation for stress/strain distribution and microstructural evolution in 42CrMo steel during hot upsetting process. *Computational Materials Science*. 2008; 43(4):1117-1122. http://dx.doi.org/10.1016/j.commatsci.2008.03.010
4. Lin YC, Chen MS and Zhong J. Prediction of 42CrMo steel flow stress at high temperature and strain rate. *Mechanics Research Communications*. 2008; 35(3):142-150. http://dx.doi.org/10.1016/j.mechrescom.2007.10.002
5. Lin YC, Chen MS and Zhong J. Application of neural networks to predict the elevated temperature flow behavior of a low alloy steel. *Computational Materials Science*. 2008; 43(4):752-758. http://dx.doi.org/10.1016/j.commatsci.2008.01.039

6. Lin YC, Chen MS and Zhong J. Study of static recrystallization kinetics in a low alloy steel. *Computational Materials Science*. 2008; 44(2):316-321. http://dx.doi.org/10.1016/j.commatsci.2008.03.027

7. Kim SI, Lee Y and Byon SM. Study on constitutive relation of AISI 4140 steel subject to large strain at elevated temperatures. *Computational Materials Science*. 2003; 140(1-3):84-89.

8. Lin YC, Chen MS and Zhong J. Microstructural evolution in 42CrMo steel during compression at elevated temperatures. *Computational Materials Science*. 2008; 62(14):2132-2135.

9. Kim SI and Yoo YC. Prediction of dynamic recrystallisation behaviour of AISI type 4140 medium carbon steel. *Materials Science and Technology*. 2002; 18(2):160-164. http://dx.doi.org/10.1179/026708301125000375

10. Quan GZ, Li GS, Chen T, Wang YX, Zhang YW and Zhou J. Dynamic recrystallization kinetics of 42CrMo steel during compression at different temperatures and strain rates. *Materials Science and Engineering A*. 2011; 528(13-14):4643-4651. http://dx.doi.org/10.1016/j.msea.2011.02.090

11. Zheng QG, Ying T and Jie Z. Dynamic softening behaviour of AZ80 magnesium alloy during upsetting at different temperatures and strain rates. *Proceedings of the Institution of Mechanical Engineers, Part B*: Journal of Engineering Manufacture. 2010; 224(11):1707-1716. http://dx.doi.org/10.1243/09544054JEM1965

12. Mandal S, Mishra SK, Kumar A, Samajdar I, Sivaprasad PV, Jayakumar T et al. Evolution and characterization of dynamically recrystallized microstructure in a titanium-modified austenitic stainless steel using ultrasonic and EBSD techniques. *Philosophical Magazine*. 2008; 88(6):883-897. http://dx.doi.org/10.1080/14786430801989799

13. Mandal S, Bhaduri AK and Sarma VS. A study on microstructural evolution and dynamic recrystallization during isothermal deformation of a Ti-modified austenitic stainless steel. *Metallurgical and Materials Transactions*. 2011; 42(4):1062-1072. http://dx.doi.org/10.1007/s11661-010-0517-7

14. Mandal S, Bhaduri AK and Sarma VS. Influence of state-of-stress on dynamic recrystallization in a Ti-modified austenitic stainless steel. *Metallurgical and Materials Transactions*. 2012; 43(2):410-414. http://dx.doi.org/10.1007/s11661-011-1015-2

15. Mandal S, Sivaprasad PV and Sarma VS. Dynamic recrystallization in a Ti modified austenitic stainless steel during high strain rate deformation. *Materials and Manufacturing Processes*. 2010; 25(1-3):54-59. http://dx.doi.org/10.1080/10426910903162985

16. Mandal S, Bhaduri AK and Sarma VS. Role of twinning on dynamic recrystallization and microstructure during moderate to high strain rate hot deformation of a Ti-modified austenitic stainless steel. *Metallurgical and Materials Transactions*. 2012; 43(6):2056-2068. http://dx.doi.org/10.1007/s11661-011-1012-5

17. Imbert CAC and McQueen HJ. Dynamic recrystallization of A2 and M2 tool steels. *Materials Science and Engineering A*. 2001; 313:104-116. http://dx.doi.org/10.1016/S0921-5093(01)00974-1

18. Salvatori I, Inoue T and Nagai K. Ultrafine grain structure through dynamic recrystallization for Type 304 stainless steel. *ISIJ International*. 2002; 42:744-750. http://dx.doi.org/10.2355/isijinternational.42.744

19. Mao PL, Su GY and Yang K. Dynamic recrystallisation of as cast austenite in 18-8 stainless steel. *Materials Science and Technology*. 2002; 18:892-896. http://dx.doi.org/10.1179/026708302225004793